



SOLIDS DEPOSITION IN LIQUIDS PETROLEUM (OIL) AND WET-GAS PIPELINES FOR INTERNAL CORROSION PREDICTIVE MODELING (ICPM)

Zhenjin Zhu, Keith W. Sand, Patrick J. Teevens
Broadsword Corrosion Engineering, Ltd.

Copyright 2010 NACE International

Requests for permission to publish this manuscript in any form, in part or in whole must be in writing to NACE International, Publications Division, 1440 South Creek Drive, Houston, Texas 77084-4906.

The material presented and the views expressed in this paper are solely those of the author(s) and not necessarily endorsed by the Association. Printed in Canada

SOLIDS DEPOSITION IN LIQUIDS PETROLEUM (OIL) AND WET-GAS PIPELINES FOR INTERNAL CORROSION PREDICTIVE MODELING (ICPM)

Zhenjin Zhu, Keith W. Sand, Patrick J. Teevens

Broadsword Corrosion Engineering, Ltd.
90 Commercial Drive, Calgary, Alberta, Canada, T3Z 2A7

ABSTRACT

This paper conducted a numerical study to track particle trajectories and to further characterize solids deposition behaviours in liquids petroleum (oil) and wet-gas pipelines. In this study, velocity fields of single-phase liquids petroleum flow were determined from empirical formulae. The liquid-phase velocity distributions in gas-liquid multiphase flow such as stratified smooth/wavy flow, slug flow, elongated/dispersed bubble flow, and annular mist flow were numerically computed by writing in-house codes or using commercial software. Based on the acquired liquid velocity fields, particle velocities were calculated from Newton's second law, and particle trajectories were tracked by solving the motion equation using the fourth-order Runge-Kutta method. With an approximate wall effect, solids deposition amount along petroleum pipelines was quantified. Furthermore, solids deposition behaviours with respect to pipeline terrain, particle properties, liquid viscosity, and flow rates were characterized.

Keywords: Numerical study, Single-phase liquids petroleum (oil) flow, Multiphase oil-gas flow, Particle trajectory, Solids deposition, Internal corrosion predictive model (ICPM)

INTRODUCTION

The presence of sand in petroleum pipelines has presented a range of challenges to the petroleum industry. When solids travel in a pipeline system, they increase pressure drawdown, restrict the quantity of the oil withdrawn from the reservoir, and cause the erosion of equipment. Fine sands absorb inhibitor and thus deplete the inhibitor species resulting in less inhibitor filming on the internal surfaces of the pipeline and related facilities, whereas coarse sands disturb the hydrodynamic boundary layer as well as the passive films. Furthermore, the deposited sands can trigger under-deposit pitting corrosion, leading to eventual pipeline failures [1-7]. Currently, about 70% of the world's total hydrocarbons are located in poorly consolidated reservoirs. Most petroleum pipelines have a volumetric concentration of sands ranging from 1% to 40%. Unless removed and cleaned regularly, sands and other solids in the production fluid will settle on the bottom of the pipeline, making accumulation of deposited solids inevitable [8-13]. The size of the deposits is proportional to the degree of wall loss occurring under the deposited solids, and the pits cannot expand beyond the deposits. Only if the deposited solids accumulate to a certain level can an enclosed corrosion environment be sustained long enough to perforate the petroleum pipelines. So far, many pipeline failures have been reported due to solids deposition [14-17]. An assessment is required to establish whether the system needs to be inspected prior to performing any inspection work. Hence, locating

expected solids deposition sites and predicting the size of the deposited solids are essential to improve pipeline integrity. With this knowledge the under-deposit pitting corrosion rate can be estimated as a result of the cell created between the underlying pipe and the bulk fluid above the solids as well as the diffusional gradient created by the accumulated solids with a depth and porosity within the pipeline over its subregional length.

BACKGROUND

In petroleum flow, as particles fall, the displaced fluid moves in opposite direction, slowing down the fall of the particles. As well, the fall of a particle is hindered by collision with other particles. Coagulation with other particles results in agglomerates which fall faster. Even if particles do not agglomerate, they may fall "in formation" which speeds their fall. Since solids only stay inside the liquid phase rather than the gas phase, particle trajectories strongly depend on the flow behaviours of liquids including oil, water, condensate, and inhibitors. Of course, the flow of liquids does relate to the behaviour of the gas phase inside pipelines. Interaction between gas and liquids generates a variety of flow patterns upon variations in pipeline terrain. Specifically, in a horizontal subregion, the flow separates the phases and creates stratification under the effect of gravity if the gas-phase velocity is insufficient to maintain the annulus of liquid around the circumference of the pipe. As the gas flow rate increases, a stratified wave flow appears. When the wave propagating along the interface touches the top wall of the pipe, a slug flow takes place. A dispersed flow appears at high gas velocities with the liquid phase dispersed as droplets. Higher gas flow rates will result in froth flow whereas lower gas flow rates cause bubble flow. In bubbly flow, bubbles are moving in the upper part of the pipe. As bubbles coalesce under an elevated gas flow rate, a plug flow regime emerges. With high gas flow rates and low liquid flow rates annular flow exists. In annular mist flow, the liquid phase forms an annulus around the circumference of the pipe with the gas flowing through the central core. Each flow regime will have its own specific liquid-phase velocity field, leading to totally different solids deposition behaviour [18-29].

To date, a vast amount of research has been conducted regarding the determination of flow regime. The earliest regime maps for two-phase gas-liquid flow were proposed by Baker in horizontal channels [30]. Mandhane et al. [31] constructed a flow-regime map using 5935 data points, 1789 of which concern air-water flows. Based on the general trends of Mandhane's map, Taitel and Dukler [32] developed a theoretical approach to predict transition between flow regimes. Subsequently, Hanratty [33], Prosperetti [34], Petalas and Aziz [35] addressed the mechanisms and criteria for regime transitions in fully-developed, steady-state, adiabatic pipe flows. To calculate velocity fields in gas-liquid two-phase flow, many approaches have been published including Arbitrary Lagrangian-Eulerian (ALE) [36], Level-set method [37], and Volume-of-fluid (VOF) [38]. To detect solids deposition inside petroleum pipelines, several acoustic sand detectors are commercially available [39]. Nonetheless, prediction of solids deposition amount in liquids petroleum and wet-gas pipelines still remains largely inexact.

MODELING AND METHODOLOGY

In multiphase petroleum flow, gas-liquid interfaces will be deformed, broken up, and coalesced. Tracking these interface movements is extremely complex and some part is beyond current modelling capabilities from first principles. As a first study, this paper made essential simplifications and assumptions. That is, rather than vividly tracking the evolution of free surface, this paper concentrated on understanding the solids deposition behaviours during the occurrence of flow patterns frequently encountered in petroleum pipelines such as stratified smooth/wavy flow, slug, bubble flow and annular mist flow. The petroleum flows were considered to be Newtonian and isothermal in each individual

subregion. Particle-particle interactions were neglected. The existence of solids did not affect the fluid structure.

Particle Trajectories

Based on the Lagrangian approach, the motion of particles is governed by the following kinetic equation:

$$\frac{d\bar{\mathbf{x}}_p}{dt} = \bar{\mathbf{u}}_p(\bar{\mathbf{x}}_p, t) \quad (1)$$

where $\bar{\mathbf{x}}_p$, t and $\bar{\mathbf{u}}_p$ represent particle position, time and particle velocity, respectively. The particle velocity was determined from Newton's Second Law. That is,

$$\sum \bar{\mathbf{F}} = m_p \frac{d\bar{\mathbf{u}}_p}{dt} \quad (2)$$

where $\sum \bar{\mathbf{F}}$ stands for the total force and m_p represents particle mass. For tiny and spherical particles, all insignificant forces such as pressure gradient, Saffman force, Magnus force, and Basset force were neglected. Thus, Eq. (2) yields

$$\rho_p \frac{d\bar{\mathbf{u}}_p}{dt} = (\rho_f - \rho_p)\bar{\mathbf{g}} - \frac{3}{4d_p} \rho_f C_D (\bar{\mathbf{u}}_p - \bar{\mathbf{u}}) |\bar{\mathbf{u}}_p - \bar{\mathbf{u}}| \quad (3)$$

where ρ symbolizes the density; the subscriptions "p" and "f" denote the particle and fluid phase, respectively; \mathbf{g} is gravity; d represents particle diameter, C_D signifies the drag coefficient; and $\bar{\mathbf{u}}$ stands for liquid velocity. In this work, wall effects were considered through modifying its drag coefficient $C'_D = C_D(1 + \frac{2.1d_p}{D})$ only if $d_p > 0.01D$, where D is pipe diameter. When the solids concentration is higher enough, the density and viscosity of the resulting suspension will be larger than those of the pure liquids. An effective density of the liquid-solid mixture was obtained by $\rho_e = \rho_f + \varepsilon_e(\rho_p - \rho_f)$ and the viscosity of a suspension was updated using $\mu_e = \mu_f(1 + 2.5\varepsilon_e)$, where ε_e stands for the solids holdup and μ represents the dynamic viscosity. The drag coefficient was given by [40-43]

$$C_D = \frac{24}{\text{Re}_p}; \text{Re}_p < 0.5 \quad (4)$$

$$C_D = 0.44; \text{Re}_p > 500 \quad (5)$$

$$C_D = \frac{24}{\text{Re}_p} (1 + 0.15 \text{Re}_p^{0.687}); 0.5 \leq \text{Re}_p \leq 500 \quad (6)$$

where the particle Reynolds number $\text{Re}_p = \frac{\rho d_p |\bar{\mathbf{u}}_p - \bar{\mathbf{u}}|}{\mu}$.

If the particles were non-spherical such as corrosion product scales (FeCO_3 and FeS) and non-corrosion product mineral scales (BaSO_4 , CaCO_3 , SrSO_4 , and CaSO_4) [44], their sphericity, Φ_s , was defined by the relation

$$\Phi_s = \frac{6v_p}{d_p \cdot s_p} \quad (7)$$

where v_p denotes the particle volume, and s_p symbolizes the surface area of particle. Accordingly, the drag coefficients were modified as per the following:

$$C_D' = K_S C_D \frac{4A_p}{\pi d_p^2}; \text{Re}_p < 0.5 \quad (8)$$

$$C_D' = K_N C_D; \text{Re}_p > 500 \quad (9)$$

$$C_D' = K_N \left[\frac{24}{\text{Re}_G} (1 + 0.1118 \text{Re}_G^{0.6567}) + \frac{0.4305}{1 + \frac{3305}{\text{Re}_G}} \right]; 0.5 \leq \text{Re}_p \leq 500 \quad (10)$$

where the generalized particle Reynolds number $\text{Re}_G = \text{Re}_p \frac{K_N}{K_S}$. In turn, $K_S = \frac{1}{3} \left(1 + \frac{2}{\sqrt{\Phi_s}}\right)$ and

$$\log_{10} K_N = 1.8148 \times (-\log_{10} \Phi)^{0.5743}.$$

Liquid-Phase Velocity

Single-Phase Liquids Petroleum Flow: In this context, empirical formulae were applied to determine the velocity distribution of single-phase liquids petroleum flow. Specifically, for fully developed turbulent flow, the velocity profile was expressed as [45]

$$\frac{U}{U_{\max}} = \left(\frac{r_0 - r}{r_0}\right)^m \quad (11)$$

where U_{\max} , r , r_0 , and m represent the maximum velocity, distance to the centerline, pipe radius, and the exponent for the power-law equation respectively. The parameters have been summarized in Table 1. Similarly, the following empirical formula was applied to describe velocity distribution of single-phase laminar flow [45]. Namely,

$$\frac{U}{U_{\max}} = \frac{r_0^2 - r^2}{r_0^2} \quad (12)$$

Gas-Liquid Two-Phase Flow: Velocity distribution of liquid phase in gas-liquid two-phase flow was numerically simulated by writing in-house codes to solve the following continuity and momentum equations:

$$\nabla \cdot \bar{\mathbf{u}} = 0 \quad (13)$$

$$\rho \frac{\partial \bar{\mathbf{u}}}{\partial t} + \rho (\bar{\mathbf{u}} \cdot \nabla) \bar{\mathbf{u}} = -\nabla p + \mu \nabla^2 \bar{\mathbf{u}} + \rho \bar{\mathbf{f}} \quad (14)$$

where p and $\bar{\mathbf{f}}$ represent the pressure and body force, respectively. In consideration of topological complexities, the Galerkin weighted residual method was employed [46] to derive their variational formula of the partial differential equations as well as the corresponding boundary values. The quadratic triangular elements and the Taylor-Hood \mathbf{P}_2 - \mathbf{P}_1 velocity-pressure scheme were applied to generate the mesh of the computational domain. A “pressure-splitting” approach [47] was utilized to solve for the momentum equations. For the cases of turbulent flow or complicated geometry, commercial software was utilized. In addition, through an analytical derivation, the following velocity profile was applied to describe the velocity in the liquid film associated with annular mist flow:

$$u(y) \approx \frac{y}{\delta} \cdot u_{\delta} \quad (15)$$

where u_{δ} represents the liquid velocity at gas-liquid interface with a film thickness of δ . It equals the average gas-phase velocity. Table 2 summarizes the approaches to determine the velocity fields of liquid phase in gas-liquid multiphase flow.

RESEARCH CONTENTS

Particle Trajectories and Solids Deposition in Single-Phase Liquids Petroleum Flow

Particle Trajectories in a Horizontal Subregion: Figure 1 illustrates the global trajectories of particles in a horizontal subregion fully occupied by liquids petroleum. In this case, the pipe diameter was 30 cm. The liquids had a kinetic viscosity of 1.0×10^{-5} m²/s and an average flow velocity of 1.0 m/s. The particles were assumed to be distributed homogenously in the pipe with a radius of 250 μ m and a density of 2500 kg/m³. It is noted that the maximum distance which the particle can travel is 1024 m.

Quantification of Solids Deposition in a Horizontal Subregion: To quantify solids deposition behaviour, the percentage of solids deposition amount (G) within a certain distance was defined as the number of deposited particles ($n_{\text{Deposited}}$) divided by the total particle number (n_{Total}) at the pipe inlet. Namely,

$$G = \frac{n_{\text{Deposited}}}{n_{\text{Total}}} \times 100\% \quad (16)$$

Using the simulated particle trajectories in Figure 1, solids deposition amount as a function of distance was quantified in Figure 2. Through polynomial fitting, the global distribution of solids deposition in a horizontal pipeline was formulated as follows:

$$G(L) = A_0 + A_1 \times \left(\frac{L}{L_{\max,0}}\right) - A_2 \times \left(\frac{L}{L_{\max,0}}\right)^2 + A_3 \times \left(\frac{L}{L_{\max,0}}\right)^3 - A_4 \times \left(\frac{L}{L_{\max,0}}\right)^4 \quad (17)$$

where A_0 , A_1 , A_2 , A_3 and A_4 are the fitting parameters; L signifies the distance from the position to the pipe inlet; and $L_{\max,0}$ stands for the maximum travelling distance. The solids deposition amount between two arbitrary sites was described by

$$\Delta G|_{L_1}^{L_2} = G(L_2) - G(L_1) \quad (18)$$

Given a volumetric concentration of suspended sands at the pipeline inlet, the number of particles deposited between two sites over a time interval was obtained from

$$\Delta N|_{L_1}^{L_2} = \frac{C_v \cdot Q}{\rho_p \cdot v_p} \cdot \Delta G|_{L_1}^{L_2} \times \Delta t \quad (19)$$

where C_v and Q represent solids concentration and volumetric discharge flow rate respectively. When a volumetric packing limit of solids particles in the granular bed was assigned, the thickness of the deposited solids could be determined.

Effects of Solids/Liquids Properties and Pipeline Geometry on Solids Deposition: To understand the effects of particle properties, liquids parameters, and pipeline geometry on solids deposition behaviours, the following cases were investigated. Figure 3 illustrates the effect of particle density on solids deposition amount by fixing the particle radius at 250 μ m, the kinetic viscosity of liquid at 1.0×10^{-5} m²/s, and the average flow velocity at 1.0 m/s. Figure 4 demonstrates variation of solids deposition

amount with respect to liquid viscosity when particle radius, particle density, and average flow velocity were retained at 250 μm , 5000 kg/m^3 , and 1.0 m/s , respectively. Figure 5 describes the influence of particle radius on solid deposition amount using a particle density of 5000 kg/m^3 , a kinetic viscosity of $1.0 \times 10^{-5} \text{ m}^2/\text{s}$, and an average velocity of 1.0 m/s . Figure 6 illustrates the solids deposition amount as a function of average flow velocity by fixing the particle radius, particle density, and kinetic viscosity at 250 μm , 5000 kg/m^3 , $2.0 \times 10^{-6} \text{ m}^2/\text{s}$, respectively. It was observed that a large and dense particle tends to deposit quickly in liquids with a low viscosity and flow rate. In addition, a larger pipe can carry particles a longer distance.

Consequently, when particles are homogeneously distributed, solids deposition amount with respect to particle density and radius, liquid viscosity, flow rate, inclined angle, and pipe diameter in a single-phase liquids petroleum flow can be predicted through updating the maximum traveling distance as the followings:

$$L_{\max}(\rho, r_p, U_{ave}, \nu, \theta, D) = L_{\max,0} \times \frac{L(\rho)}{L_{\rho,0}} \times \frac{L(r_p)}{L_{r_p,0}} \times \frac{L(\nu)}{L_{\nu,0}} \times \frac{L(U_{ave})}{L_{U_{ave},0}} \times \frac{L(\theta)}{L_{\theta,0}} \times \frac{L(D)}{L_{D,0}} \quad (20)$$

where $L(\rho)$, $L(r_p)$, $L(\nu)$, $L(U_{ave})$, $L(\theta)$ and $L(D)$ are the functions of particle density, radius, liquid viscosity, average velocity, inclined angle, and pipe diameter on the maximum traveling distance. In turn, $L_{\rho,0}$, $L_{r_p,0}$, $L_{\nu,0}$, $L_{U_{ave},0}$, $L_{\theta,0}$, and $L_{D,0}$ represent the maximum traveling distances of these base cases.

Particle Trajectories in Multiphase flow

Stratified Smooth Flow: Stratified flow occurs in the horizontal and downhill subregions. It includes stratified smooth flow and stratified wavy flow. Figure 7 illustrates 2-D velocity distribution of stratified smooth flow which flows in a horizontal subregion with a liquid height of 0.08 m, length of 1 m, dynamic viscosity of 0.02 $\text{kg}/\text{m}\cdot\text{s}$, density of 850 kg/m^3 , and average gas velocity of 1.0 m/s . In this case, a non-slip boundary condition was applied at the bottom whereas a Dirichlet boundary condition was assigned at the top. The pressure difference between the inlet and the outlet is 20 Pa. It is revealed that, driven by the shear stress at the gas-liquid interface, the liquid has a maximum velocity at the top. The velocity diminishes quickly deeper into the liquid layer. Based on the calculated velocity distribution of the liquids, particle trajectories were tracked. As demonstrated in Figure 8, the particles close to the bottom will deposit very quickly.

Stratified Wavy Flow: With the presence of waves at the gas-liquid interface, stratified wavy flow appears. Similarly, a non-slip boundary condition was applied at the bottom whereas Dirichlet boundary conditions were assigned at the free surface with a constant velocity along the tangential direction. Figure 9 depicts the velocity distribution of stratified wavy flow in a horizontal subregion when a sine wave has an amplitude of 50% of average liquid height, an average liquid height of 0.08m, liquid kinematic viscosity of $5 \times 10^{-6} \text{ m}^2/\text{s}$, liquid density of 850 kg/m^3 , pressure drop of 20 Pa, interfacial velocity of 1.0 m/s , and a subregion length of 1 m. It can be seen that a recirculation zone exists under the wave peak. As the wave amplitude decreases, the vortex diminishes.

Figure 10 displays trajectories of particles with a radius of 200 μm and density of 2500 kg/m^3 in stratified wavy flow. It is found that beneath the wavy peak, more solids will be suspended and circulated inside the recirculation zone. Under the wave valley, there is a large shear stress which tends to sweep solids forward. Thus, fewer solids will be deposited in stratified wavy flow as compared to stratified smooth flow. In addition, the wavy peak and valley appear alternatively with a certain frequency. Such a periodical suspension and sweeping makes solids deposition difficult to achieve in certain locations. Since under-deposit pitting corrosion requires an incubation time to build up and

maintain the corrosive environment, the probability of pitting corrosion occurring under the deposited solids will decrease as wavy strength increases.

Slug Flow: When the wave peak hits the top of the pipe, slug flow results. In slug flow, the entire pipe is occupied by a liquid slug and a gas pocket. A precise numerical study of slug flow is overwhelmingly complicated due to turbulent deformation, break-up and coalescence of free surfaces at the slug front and rear. To understand the impact of slug flow on solids deposition behaviours (i.e., role of gas pocket in the existing slug flow on particle trajectories), this work simulated a simple example of slug flow which occurred in an uphill subregion. In this case, the pipe diameter was 15 cm, liquid kinematic viscosity was 5×10^{-6} m²/s, and liquid density was 850 kg/m³. The height of the gas pocket was designed to be 50% of the pipe diameter, and the pressure drop between the inlet and outlet was 20 Pa. During numerical simulation, non-slip conditions were applied at the bottom as well as the top where the liquid touches the top of pipe. The gas pocket was assumed to be rigid with a thin solid film at the interface, and an empirical slug velocity was applied at the gas-liquid interface [1]. Its velocity profile was demonstrated in Figure 11. It can be seen that the existence of a gas pocket shrinks the cross-sectional area occupied by liquids. The liquids under the gas pocket behave as a 'neck' which has a thin liquid layer.

Figure 12 displays the trajectories of the particles having a density of 2500 kg/m³ and radius of 200 μm in uphill slug flow. It is observed that particles were blocked by the 'neck' and suspended in the slug flow liquid. After one slug passes, another slug follows up. The deposited particles will be swept periodically. An intensive exchange of particles between the stationary layer and the moving slug will take place. Few particles will be accumulated in any given location for an extended period of time. Thus, under-deposit corrosion will not occur in slug flow. Nonetheless, slug flow will promote general corrosion because impingement of solid particles on the metal surface will peel off and remove the scale. Due to an intermittent pattern of alternating flow supply and pressure along the pipeline, the interaction between the slug liquid and the gas pocket can create serious operational upsets.

Elongated Bubble Flow: Bubble flow can be either elongated bubble flow or dispersed bubble flow. To simulate elongated bubble flow a 2-D Finite Element Method was applied. Specifically, a non-slip boundary condition was assigned at the bottom and the top metal surface where it contacted the liquid. The gas-liquid interface was considered to be rigid with an elongated bubble velocity which was empirically determined [1]. Figure 13 plots the velocity profile of elongated bubble flow in an uphill subregion with a pipe diameter of 0.15 m, length of 1 m, and inclined angle of +5°. The flow has a liquid kinematic viscosity of 5×10^{-6} m²/s, liquid density of 850 kg/m³, elongated velocity of 0.1 m/s, and pressure drop of 20 Pa. Existence of an elongated bubble reduces the liquid occupied area and generates a 'neck' liquid layer. Figure 14 shows trajectories of the particles having a radius of 200 μm and a density of 2500 kg/m³ in elongated bubble flow. Particles were blocked due to the existence of the bubble. As the shrinkage ratio of liquid occupied area increases, more solids will be settled.

Dispersed Bubble Flow: Dispersed bubble flow has a great number of tiny bubbles. These bubbles tend to stay on the upper part of the pipe. In this study, Finite-Element-Method-based commercial software was applied to generate the mesh as well as to estimate the liquid velocity. Figure 15 demonstrates the velocity distribution of bubbly flow. It shows that the existence of tiny bubbles reduces the effective liquid velocity at the bubble zone. The actual height occupied by the liquid phase is decreased. Figures 16 (a) and (b) depict the trajectories of particles with different density and size. As expected, large and dense particles will deposit early.

Annular Mist Flow: As aforementioned, an analytical solution was derived to approximate the velocity profile inside the liquid film of annular mist flow. Based on the velocity distribution in the liquid film, the particle trajectories were approximated. Figure 17 illustrates the effect of film thickness on solids deposition amount. In this case the following parameters were used: average gas velocity 15 m/s, particle density 2500 kg/m³, particle radius 200 μm, and the liquid kinematic viscosity 5×10^{-6} m²/s. A thin liquid film leads to a shorter particle travelling distance. Figure 18 plots that the effect of pipeline

terrain on solids deposition amount. It is indicated that solids are prone to settle in downhill sections in comparison to uphill sections under a low velocity.

Solids Deposition Amount in Multiphase Flow

Solids deposition amount in multiphase flow was quantified based on the developed approach used for single-phase petroleum flow. Since particle trajectories and maximum travelling distance strongly depend on the height of the liquid layer, an effective height of the liquid occupied area was calculated first. It was determined in terms of the shrinkage ratio of liquid occupied area which was defined as

$$\Phi = \frac{A - A_g}{A} \quad (21)$$

where A and A_g denote the pipe cross-sectional area and gas-phase occupied area respectively. As well, the average velocity of the liquid phase was estimated using

$$V_{ave} = \frac{Q}{\Phi \cdot A} \quad (22)$$

where Q stands for the liquid flow rate.

To verify this model, the model results were compared to a real case (a 4" production group line owned by a client in California). In this pipeline, the fluid temperature was 22 °C and the internal gauged pressure was 3.44653 bar. The pipeline had an external diameter 88.9 mm, pipe thickness of 5.41 mm, and pipe roughness of 0.08 mm. The oil and condensate flow rate was 22.061 m³/day; the gas flow rate [STP] was 351 m³/day; water flow rate was 206.317 m³/day. The API gravity of the oil/condensate was 37.31 and the ambient temperature was 30 °C. The particle density was 2000 kg/m³ and particle radius was 100 μm. Results in Figure 19 demonstrate that a significant amount of solids had been deposited at a distance of 396.2 m from the pipeline inlet. Since this line had indeed failed at this precise location, it can be said that the model agrees well with practical data.

As well, it can be said that solids tend to settle in the upstream areas. This is because each particle has a maximum travel distance which varies depending on initial particle position, density, and so on. Only under extreme conditions (e.g. particles having a very low density and a small size), can the solids arrive at the end of pipeline. Since solids density in petroleum pipelines range from 1500 kg/m³ to 5000 kg/m³, most particles will settle before they reach the end. In addition, solids are prone to settle in downhill subregions instead of uphill subregions. The reason is that the flow regime in uphill locations is often slug flow whereas stratified flow occurs in downhill areas. In slug flow, the solids bed was periodically swept by slug liquid resulting in more suspended solids. However, in stratified flow, a decreased thickness liquid layer reduces the maximum travel distance of any suspended particles. As a consequence, more solids will be deposited in downhill locations than in uphill locations. In addition, more under-deposit pitting corrosion will be expected to happen in the stratified and elongated flow regimes than in the slug flow and annular mist flow regimes. The reason is that stratified flow has a thin liquid layer, and the elongated flow regime has a low liquid flow rate. Although annular mist flow has a thinner liquids film, it commonly occurs further downstream. Due to flow resistance, the pressure downstream is decreased. Under low pressure gas will expand which decreases liquids holdup and height. Most particles have settled before the downstream portions of the pipeline are reached. In addition, there is strong convection associated with a high gas velocity in annular mist flow, which makes it difficult to maintain a corrosive environment under the deposited solids.

CONCLUSION

This paper numerically studied the solids deposition behaviours in liquid petroleum (oil) and wet-gas pipelines for internal corrosion predictive modeling (ICPM). The effects of particle properties, liquid viscosity, flow rates, and pipeline geometry on solids deposition behaviours were characterized. The effective thickness of liquid layer is a crucial parameter on determining maximum travel distance of particles. Solids tend to deposit upstream in downhill subregions experiencing shallow stratified smooth flow.

ACKNOWLEDGEMENT

The authors are grateful to the financial support of the Alberta Ingenuity Funds.

REFERENCES

1. Lyons WC, Plisga GJ, Standard handbook of petroleum and natural gas engineering, Second edition, Elsevier Inc., 2005.
2. Sand K, Deng C, Teevens PJ, Predictive modeling of the internal corrosion of sweet and sour multiphase pipelines, Paper 53, Australian Corrosion Association Corrosion & Prevention, 2005.
3. Deng C, Sand K, Teevens PJ, A web based software for prediction of the internal corrosion of sweet and sour multiphase pipelines, Paper 06565, Corrosion NACEExpo, 2006.
4. Zhu Z, Sand KW, Teevens PJ, Studies of solids deposition and under-deposit pitting corrosion in liquids petroleum pipelines, Paper 20, Australian Corrosion Association Corrosion & Prevention, 2009.
5. Uhlig HH, Corrosion handbook, John Wiley & Sons, Inc., New York, 1948.
6. Fontana MG, Corrosion engineering, McGraw-Hill Inc., 1986.
7. Marcus P, Corrosion mechanisms in theory and practice, Second Edition, Marcel Dekker, Inc., New York, 2002.
8. Abass HH, Nar-EI-Din HA, BaTaweel MH, Sand control: sand characterization, failure mechanisms, and completion methods, SPE paper 77686, San Antonio, Texas, 2002.
9. Geilikman MB, Dusseault MB, Dullien FA, Sand production as a viscoplastic granular flow, SPE paper #27343, Lafayette, Louisiana, 1994.
10. Morita N, Boyd PA, Typical sand production problems: Case studies and strategies for sand control, SPE paper 22739, Dallas, TX, 1991.
11. Nouri A, Vaziri H, Belhaj H, Islam R, Comprehensive transient modeling of sand production in horizontal wellbores, SPE Paper 84500, Denver, Colorado, 2003.
12. Almedeij JH, Algharaib MK, Influence of sand production on pressure drawdown in horizontal wells: Theoretical evidence, J. Pet. Sci. Eng., 47 (2005) 137-145.
13. Li J, Webb C, Pandiella SS, Campbell GM, Dyakowski T, Cowell A, McGlinchey D, Solids deposition in low-velocity slug flow pneumatic conveying, Chem. Eng. Process., 44 (2005) 167-173.
14. Isakovich I, Villalba R, Barrios C, et al., Evaluation of the internal corrosion and the solids depositions problematic in the compression plants located in the east part of Venezuela, NACE Corrosion 2006, Paper # 06371.
15. Howell AG, Under-deposit corrosion mechanisms in boilers, NACE Corrosion 2006, Paper #06548.
16. Howell AG, Under-deposit corrosion at weld seams in carbon steel piping, NACE Corrosion 1997, Paper #447.
17. Catalan LJJ, Jamaluddin AKM, Solids problem at the ring border gas plant, J. Can. Pet. Technol., 37 (1998) 46-55.
18. Barnea D, Shoham O, Taitel Y, Flow pattern transition for downward inclined two phase flow, Horizontal to vertical, Chem. Eng. Sci., 37 (1982) 735-740.
19. Cook M, Behnia M, Slug length prediction in near horizontal gas-liquid intermittent flow, Chem. Eng. Sci., 11 (2005) 2009-2018.

20. Duckler AE, Hubbard MG, A model for gas-liquid slug flow in horizontal and near horizontal tubes, *Ind. Engng. Chem. Fundam*, 14:3 (1975) 337-347.
21. Fagundes JR, Netto J, Fabre J, Peresson L, Shape of long bubbles in horizontal slug flow, *Int. J. Multiphase Flow*, 25:6/7 (1999) 1129-1160.
22. Paglianti A, Giona M, Soldatp A, Characterization of subregimes in two-phase slug flow, *Int. J. Multiphase Flow*, 22:4 (1996) 783-796.
23. Van Hout R, Shemer L, Barnea D, Evolution of hydrodynamic and statistical parameters of gas-liquid slug flow along inclined pipes, *Chem. Eng. Sci.*, 58:1 (2003) 115-133.
24. Stapelberg HH, Mewes D, The pressure loss and slug frequency of liquid-liquid-gas slug flow in horizontal pipes, *Int. J. Multiphase Flow*, 20:2, (1994) 285-303.
25. Kadri U, Zoeteweyj ML, Mudde RF, Oliemans RVA, A growth model for dynamic slugs in gas-liquid horizontal pipes, *Int. J. Multiphase Flow*, 35 (2009) 439-449.
26. Jepson WP, Taylor R E, Slug flow and its transitions in large-diameter horizontal pipes, *Int. J. Multiphase Flow*, 19 (1993) 411-420.
27. Vlachos NA, Paras SV, Karabelas AJ, Prediction of holdup, axial pressure gradient and wall shear stress in wavy stratified and stratified/atomization gas/liquid flow, *Int. J. Multiphase Flow*, 25 (1999) 365-376.
28. Tribbe C, Muller-Steinhagen HM, An evaluation of the performance of phenomenological models for predicting pressure gradient during gas-liquid flow in horizontal pipelines, *Int. J. Multiphase Flow*, 26 (2000) 1019-1036.
29. Ouyang LB, Aziz K, Transient gas-liquid two-phase in pipes with radial influx or efflux, *J. Petroleum. Sci and Eng.*, 30 (2001) 167-179.
30. Baker O, Simultaneous flow of oil and gas, *Oil Gas J*, 53 (1954) 185-190.
31. Mandhane, JM, Gregory, GA, Aziz, K, A flow pattern map for gas-liquid flow in horizontal pipes: Predictive models, *Int. J. Multiphase Flow*, 1 (1974) 537-533.
32. Taitel Y, Dukler AE, A model for predicting flow regime transitions in horizontal and near horizontal gas-liquid flow, *AIChE J.*, 22 (1976) 47-55.
33. Hanratty TJ, Theofanous T, Delhaye JM, et al., Workshop findings, *Int. J. Multiphase Flow*, 29:7 (2003)1047-1059.
34. Prosperetti A, Tryggvason G, Appendix 3 Report of study group on computational physics, *Int. J. Multiphase Flow*, 29:7 (2003) 1089–1099.
35. Petalas N, Aziz K, A mechanistic model for multiphase flow in pipes, 49th annual corrosion technical meeting of the petroleum society, Calgary, Alberta, Canada, 1998, Paper # 98-39.
36. Li J, Hesse M, Ziegler J, Woods AW, An arbitrary Lagrangian Eulerian method for moving-boundary problems and its application to jumping over water *J. Comput. Phys.*, 208 (2005) 289-314.
37. Osher S, Sethian JA, Fronts propagating with curvature-dependent speed: Algorithms based on Hamilton-Jacobi formulations, *J. Comput. Phys.* 79 (1988) 12–49.
38. Hirt CW, Nichols BD, Volume of fluid (VOF) method for the dynamics of free boundaries, *J. Comput. Phys.*, 39:1 (1981) 201-225.
39. Shirazi SA, McLaury BS, Ali MM, Sand monitor evaluation in multiphase flow, Paper # 00084, 2000.
40. Cliff R, Grace JR, Weber ME, Bubbles, drops, and particles, Academic Press NY, 1978.
41. Ahmed T, Reservoir Engineering Handbook, Elsevier, 2001.
42. Haider A, Levenspiel O, Drag coefficient and terminal velocity of spherical and nonspherical particles, *Powder Technol.*, 58 (1989) 63-70.
43. Dedegil MY, Drag coefficient and settling velocity of particles in non-Newtonian suspensions, *Intl. Symp. on Slurry Flows*, ASME Vol. FED-38 (1986): 9-15.
44. Cowan JC, Weintritt DJ, Water-formed scale deposits, Gulf Publishing Company, 1976.
45. Crowe CT, Roberson JA, Elger DF, Engineering Fluid Mechanics, John Wiley & Sons, Inc., New York, 2001.
46. Chung TJ, Computational Fluid Dynamics, Cambridge University Press, 2002.
47. Zhu Z, Wang J, James DF, Park CB, Finite element analysis of shear-thinning flow of polymer-gas solution in a hyperbolic convergent slit die, PPS-2007 Regional conference, Shanghai, China, July 12-14, 2007.

TABLE 1:
EXPONENTS FOR POWER-LAW EQUATION AND VELOCITY RATIO

Re	4×10³	2.3×10⁴	1.1×10⁵	1.1×10⁶	3.2×10⁶
M	1/6.0	1/6.6	1/7.0	1/8.8	1/10.0
U/U_{max}	0.791	0.807	0.817	0.850	0.865

TABLE 2:
APPROACHES TO DETERMINE LIQUID-PHASE VELOCITY FIELDS

Subregion	Single-Phase Flow	Gas-Liquid Multiphase Flow					
		Annular Mist	Stratified Flow		Slug Flow	Bubble Flow	
			Smooth	Wavy		Elongated	Dispersed
Horizontal	Analytic	Analytic	Numerical	Numerical	Numerical	Numerical	Commercial Software
Uphill	Analytic	Analytic	N/A	N/A	Numerical	Numerical	Commercial Software
Downhill	Analytic	Analytic	Numerical	Numerical	N/A	N/A	N/A

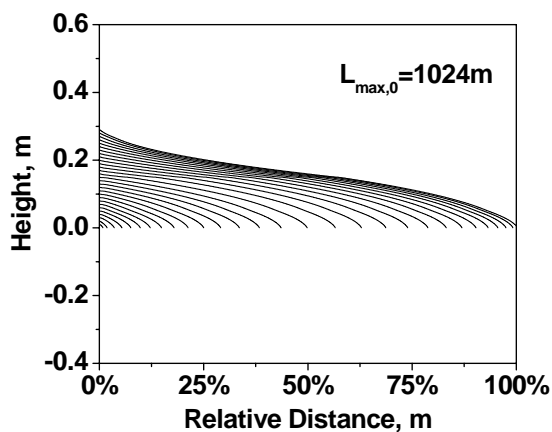


Figure 1 Trajectories of mass particles along a horizontal pipeline

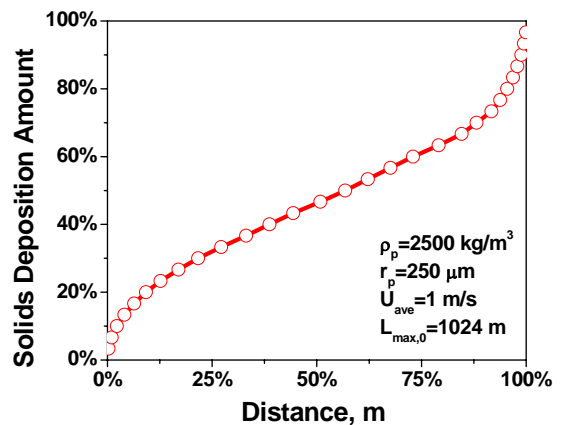


Figure 2 Solids deposition amount in a horizontal pipeline

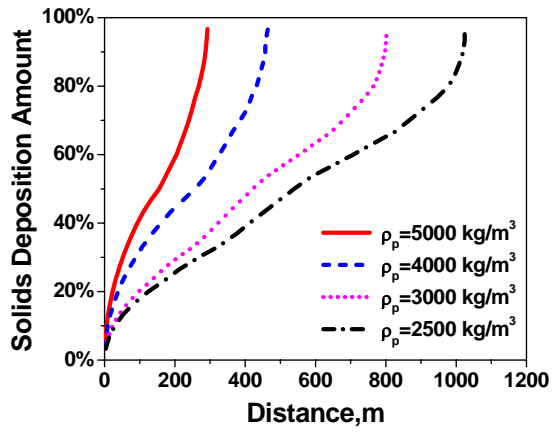


Figure 3 Effect of particle density on solids deposition amount

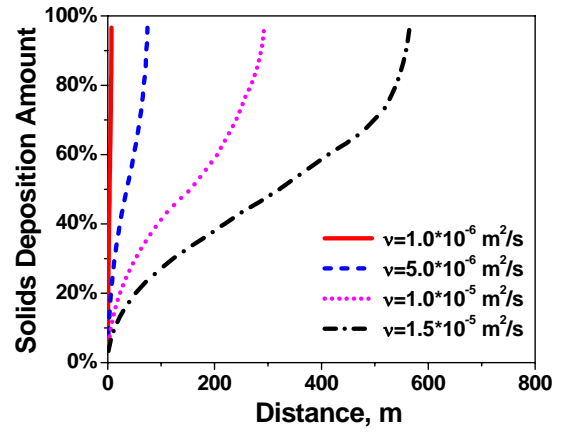


Figure 4 Effect of liquid viscosity on solids deposition amount

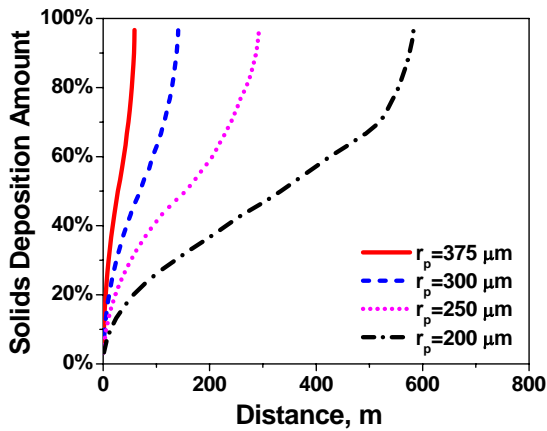


Figure 5 Effect of particle size on solids deposition amount

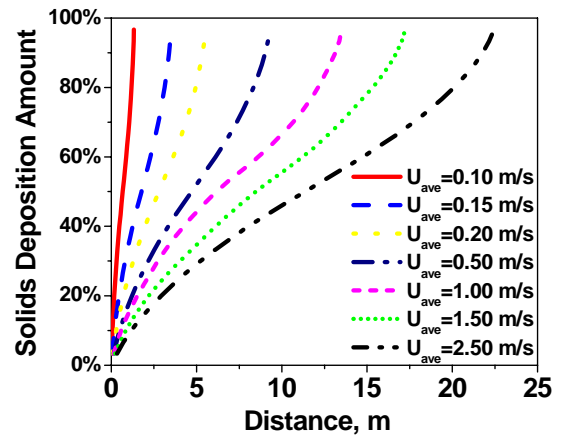


Figure 6 Effect of average velocity on solids deposition amount

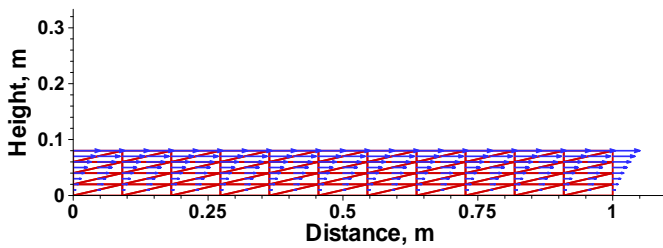


Figure 7 Velocity distribution of stratified smooth flow in a horizontal subregion

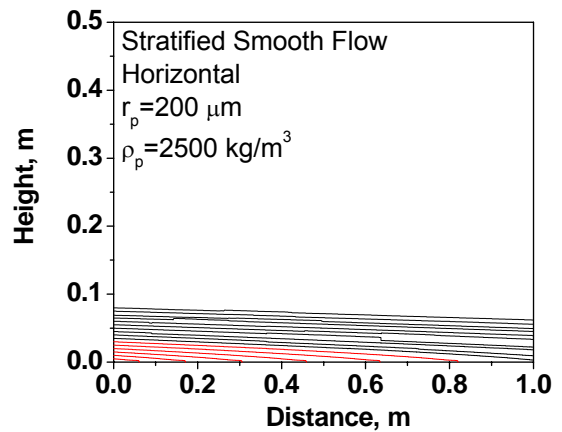


Figure 8 Particle trajectories in stratified smooth flow in a horizontal subregion

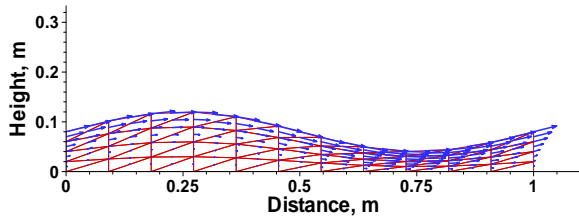


Figure 9 Velocity distribution of stratified wavy flow in a horizontal subregion

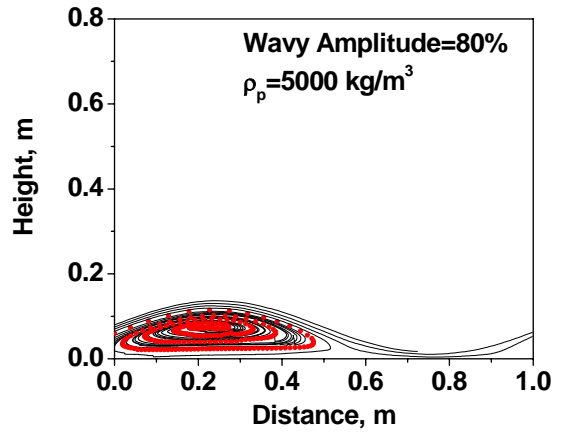


Figure 10 Particle trajectories in a stratified wavy flow in a horizontal subregion

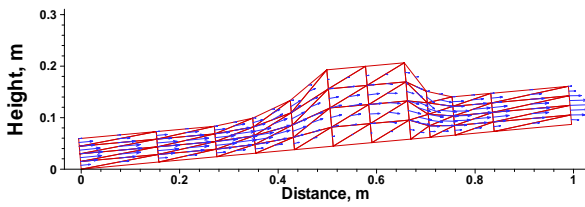


Figure 11 Velocity distribution of slug flow in an uphill subregion

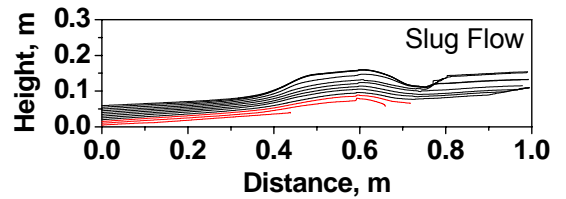


Figure 12 Particle trajectories in slug flow in an uphill subregion

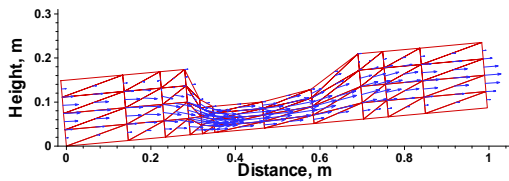


Figure 13 Velocity distribution of elongated bubble flow

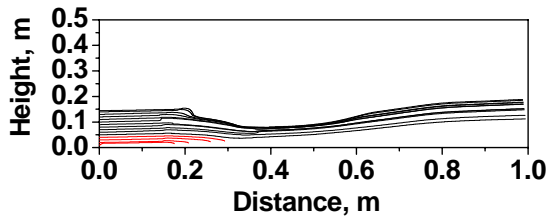


Figure 14 Solids deposition in elongated bubble flow

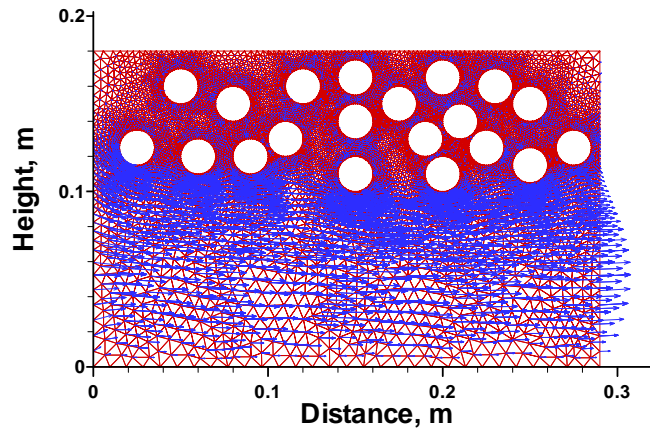
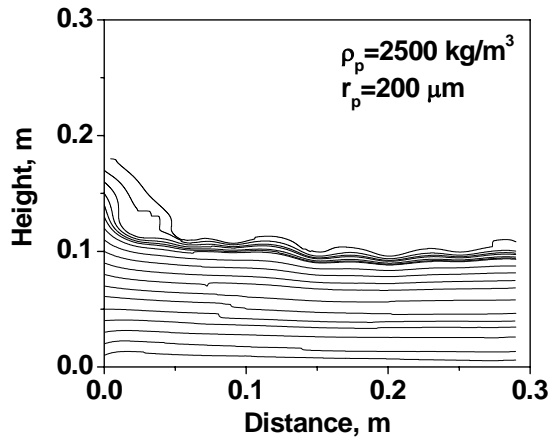
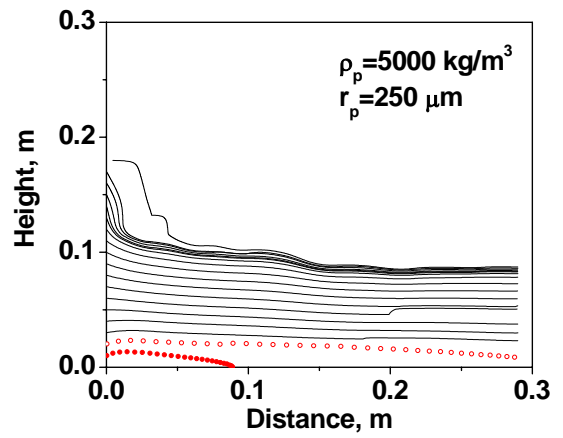


Figure 15 Mesh generation for dispersed bubble flow



(a)



(b)

Figure 16 Particle trajectories in dispersed bubble flow

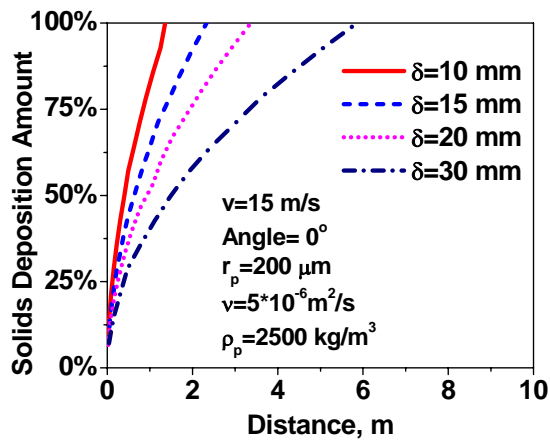


Figure 17 Solids deposition amount as a function of film thickness

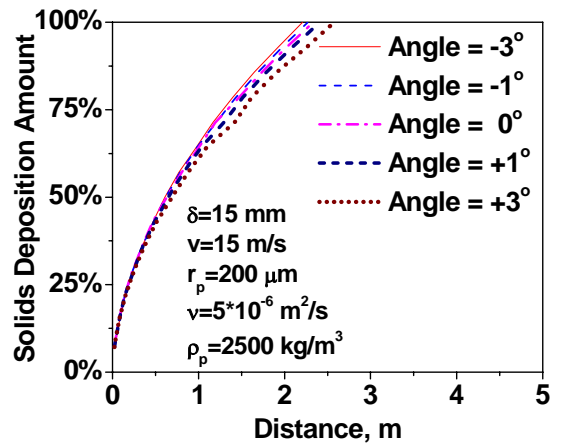


Figure 18 Solids deposition amount as a function of inclined angles

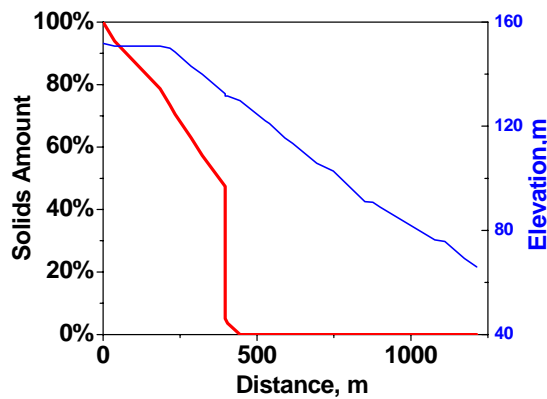


Figure 19 Solids amount along a 4'' production group line